



UNIVERSITY OF LEEDS

This is a repository copy of *Effects of skin heat conduction on aircraft icing process*.

White Rose Research Online URL for this paper:

<http://eprints.whiterose.ac.uk/169110/>

Version: Accepted Version

Article:

Shen, X, Zeng, Y, Lin, G et al. (2 more authors) (2020) Effects of skin heat conduction on aircraft icing process. Proceedings of the Institution of Mechanical Engineers, Part G: Journal of Aerospace Engineering. ISSN 0954-4100

<https://doi.org/10.1177/0954410020972577>

© IMechE 2020. This is an author produced version of an article published in Proceedings of the Institution of Mechanical Engineers, Part G: Journal of Aerospace Engineering. Uploaded in accordance with the publisher's self-archiving policy.

Reuse

This article is distributed under the terms of the Creative Commons Attribution-NonCommercial-NoDerivs (CC BY-NC-ND) licence. This licence only allows you to download this work and share it with others as long as you credit the authors, but you can't change the article in any way or use it commercially. More information and the full terms of the licence here: <https://creativecommons.org/licenses/>

Takedown

If you consider content in White Rose Research Online to be in breach of UK law, please notify us by emailing eprints@whiterose.ac.uk including the URL of the record and the reason for the withdrawal request.



eprints@whiterose.ac.uk
<https://eprints.whiterose.ac.uk/>

Effects of Skin Heat Conduction on Aircraft Icing Process

Xiaobin Shen¹, Yu Zeng¹, Guiping Lin¹, Zuodong Mu^{2,*}, and Dongsheng Wen^{1,3}

¹ School of Aeronautic Science and Engineering, Beihang University, Beijing, China

² Aviation Industry Development Research Center of China, Beijing, China

³ School of Chemical and Processing Engineering, University of Leeds, Leeds, UK

Abstract

During the aircraft icing process caused by super-cooled droplet impingement, the surface temperature and heat flux distributions of the skin would vary due to the solid substrate heat conduction. An unsteady thermodynamic model of the phase transition was established with a time-implicit solution algorithm, in which the solid heat conduction and the water freezing were analyzed simultaneously. The icing process on a rectangular skin segment was numerically simulated, and the variations of skin temperature distribution, thicknesses of ice layer and water film were obtained. Results show that the presented model could predict the icing process more accurately, and is not sensitive to the selection of time step. The latent heat released by water freezing affects the skin temperature, which in turn changes the icing characteristics. The skin temperature distribution would be affected notably by the boundary condition of the inner skin surface, the lateral heat conduction and thermal property of

* Corresponding author:

Zuodong Mu, Aviation Industry Development Research Center of China, Beijing, 100029, China. Email: muzuodong@buaa.edu.cn

the skin. It was found that the ice accretion rate of the case that the inner surface boundary is in natural convection at ambient temperature is much smaller than that with constant ambient temperature there; due to the skin lateral heat conduction, the outer skin surface temperature increases first and then decreases with uneven distribution, leading to an unsteady ice accretion rate and uneven ice thickness distribution; a smaller heat conductivity would lead to a more uneven temperature distribution and a lower ice accretion rate in most regions, but the maximum ice thickness could be larger than that of higher heat conductivity skin. Therefore, in order to predict the aircraft icing phenomenon more accurately, it is necessary to consider the solid heat conduction and the boundary conditions of the skin substrate, instead of applying a simple boundary condition of adiabatic or a fixed temperature for the outer skin surface.

Keywords

Aircraft icing; Icing thermodynamic model; Effect of heat conductivity; Ice accretion rate; Numerical simulation.

1 Introduction

When an aircraft is under icing atmospheric conditions, ice accretion due to the super-cooled droplet impingement may occur on the windward surface such as the lifting surface and engine intake lip¹, which would pose severe threat to flight safety². Ice accretion would cause the deterioration in the aerodynamic performance due to the change of aerodynamic configuration, leading to a decrease of lift and increase of

drag. It might also affect the engine performance and even cause the engine surge. In addition, ice accretion on windshields and sensors would affect the view and judgement of the pilots³. Therefore, flight accidents caused by ice accretion often occur, making up about 9 percent of all flight accidents according to the statistics from NASA⁴. In view of the serious threats that ice accretion would impose on flight safety, it is an urgent need to analyze the icing mechanism and consider the characteristics and factors of aircraft ice accretion comprehensively.

Aircraft icing is a phase change process when super-cooled droplets impinge on the skin surface, which involves mass transfer and energy exchange, and the ice accretion rate is dominated by the thermodynamic mechanism of the water film on the surface. Researchers have long noticed the threat of aircraft icing on flight safety. A large number of studies on heat and mass transfer theories and numerical simulation methods of ice accretion process have been carried out, and series of relevant software and codes were developed such as LEWICE⁵, FENSAP-ICE⁶, ONERA⁷, TRAJICE⁸, and CIRAAMIL⁹, in which various thermodynamic models were applied and among them the Messinger's model, Shallow-Water model and Myers' model were most widely adopted.

Messinger's model was presented in 1953¹⁰ and has been applied in LEWICE. The icing surface is divided into several control volumes, and the mass and energy conservation of each control volume is analyzed to establish the integrated thermodynamic equations. When super-cooled droplets impinge on icing surface, part of them freeze due to the disturbance, and the rest run back to downstream. The

relevant energy transfer terms include: the latent heat released by the water freezing, the convective heat dissipation to the air, the latent heat of water evaporation, the aerodynamic heating, and the kinetic energy of the impinging droplets¹¹. The above terms determine the ice accretion rate. Almost all of the current icing thermodynamic models are developed based on Messinger's theory. However, it assumes that skin is adiabatic, and considers only the energy transfer on the boundary of the control volume, which means the heat transfer between the water film and ice layer as well as the details of the water film runback have not been taken into account.

Based on Messinger's theory, FENSAP-ICE established Shallow-water model¹², considering the unsteady processes of water film growth, runback, and freezing. It assumes that the liquid water forms a water film on the surface of the skin or ice layer, of which the thickness would change with time and the runback water is driven by forces such as the shear stress. The energy conservation equation of water film is coupled with its momentum equation to determine the film thickness, ice accretion rate, and ice shape. To simulate ice accretion with Shallow-water model, the boundary of the outer skin surface is assumed as adiabatic, and the heat transfer between ice layer and skin has not been considered.

Myers' model¹³ refined the unsteady heat transfer and phase transition process of the water freezing on the skin surface. The aircraft skin is assumed as a fixed temperature substrate, and the latent heat of freezing transfers through water film and ice layer to the external air and the internal skin, respectively. Based on Stefan theory, unsteady Myers' thermodynamic model is established to obtain the ice accretion

characteristics of rime ice or glaze ice. Since the time discretization scheme is explicit in Myers' model¹⁴, special treatment is needed for the case of liquid water film or glaze ice at the first time step¹⁵. Based on Myers' model, researchers further added the momentum equation of the water film similar to Shallow-water model^{16,17}, and extended it to 3D calculations¹⁸. Brakel¹⁴ studied the effects of skin material on the icing process. However, the heat transfer between ice layer and skin substrate was calculated using an assumed fixed convective heat transfer coefficient, and the lateral heat conduction was not considered.

The general icing thermodynamic models discussed above focus on the water film runback and the icing process with different heat fluxes after the super-cooled droplet impingement, while the variation of the internal skin temperature distribution and its effects on the ice accretion process have not been considered. Kong¹⁹ conducted phase transition experiments of super-cooled water for icing mechanism, and found that the ice accretion process of the substrate icing was different from that of the free icing, and was affected by the heat conductivity of the substrate material. Gao²⁰ experimentally studied the ice accretion process of a wind turbine blade in icing wind tunnel, and the results showed that the ice accretion on the skin was a transient process. The skin temperature increased with time when ice accretion occurred, and the temperature change of the rime ice was different from those of the glaze ice and the mixed ice. Li²¹ conducted icing experiments with the skin materials of aluminum and thermoplastic, and analyzed the effects of the thermal conductivity of the airframe substrate on the unsteady heat transfer of the dynamic ice accretion

process. It was found that the icing process was strongly coupled with the solid skin heat conduction, and the substrate material would significantly affect the surface temperature distribution and the ice accretion characteristics. Besides the experimental studies, Morency²² applied CANICE to calculate the ice shape on a metal skin for an anti-icing system without any heat load. The simulated ice accretion rate near the end of the icing area was higher than the result which did not consider the skin heat conduction. Using Messinger's model, Shen²³ found that the lateral heat conduction of skin would affect the ice shape when conducting coupled simulation of the ice accretion and the skin heat conduction for an electro-thermal anti-icing system. Chauvin²⁴ numerically studied the influence of the normal and lateral heat conductions of the solid skin on the icing process, and compared the results obtained by ONERA model and Messinger's model. It was found that the lateral heat conduction significantly affected the ice shape of the airfoil, but the skin temperature variation and the mechanism of its effects on ice shape were not analyzed.

In general, aircraft icing process is determined by both the external ambient air-droplet conditions and the internal skin heat conduction. The thermodynamic models of current icing codes and software only focused on the heat and mass transfer at the outer side of the skin, neglecting the interaction of the solid heat conduction and the water freezing process. Studies on the temperature variation of the skin substrate and its effects on the unsteady icing process were rare. This work focuses on the effects of skin heat conduction on aircraft icing process. In the following section, the coupled unsteady ice accretion model, including the transient heat conduction of the

skin substrate and the transient icing thermodynamic model, is provided with its solution procedure. The geometry and the boundary conditions of the tested rectangular skin segment are described in Section 3. In Section 4, the established model is validated, and then the effect of the time step is checked. At the later part of this section, the effects of the normal/ lateral conduction and physical property of the skin substrate on the icing process are analyzed. The research would contribute to the improvement of aircraft icing mechanism and the development of precise numerical simulation method for aircraft icing.

2 Mathematical Models

The heat transfer of water film, ice layer, and skin substrate as well as the ice growth process are studied in this paper, while the water film flow is neglected. Considering ice accretion is an unsteady and coupled process, the transient models of the solid skin heat conduction and the water phase transition are established respectively, and then solved unsteadily in a loosely coupled method in which the outer skin surface is the data exchange interface.

2.1 Heat conduction model of skin substrate

Considering the effects of the thermal inertia and unsteady heat transfer of the skin substrate on the water freezing process, a heat conduction equation is established in the solid domain of the skin. According to Fourier's law and the conservation equation of energy, the differential equation of transient heat conduction is obtained:

$$\rho c \frac{\partial T}{\partial t} = \nabla \cdot (k \nabla T) \quad (1)$$

Where ρ is the density of the skin material, c is the specific heat capacity, T is the temperature, t is the time, and k is the heat conductivity. The boundary condition of outer skin surface is coupled with the ice layer, while the inner surface is at a constant temperature or a convective heat transfer boundary, depending on the simulation case.

In the simulations, the cell-centered finite volume method in space and the implicit difference method in time are used, as expressed as:

$$\frac{T_{m,n}^i - T_{m,n}^{i-1}}{\Delta t} = \frac{k}{\rho c} \left(\frac{T_{m+1,n}^i - 2T_{m,n}^i + T_{m-1,n}^i}{\Delta x^2} + \frac{T_{m,n+1}^i - 2T_{m,n}^i + T_{m,n-1}^i}{\Delta y^2} \right) \quad (2)$$

Where Δt is the time step, the superscript i means the value at the i -th time step, the subscripts m and n mean the cell numbers in the x -axis and y -axis directions.

2.2 Unsteady thermodynamic model of ice accretion

In view of the effect of the skin temperature variation on the water freezing process, an icing thermodynamic model is needed in which the latent heats transferred to the external air and the internal skin are included. Based on Myers' theory, the energy conservation of the unsteady icing process is shown in Figure 1.

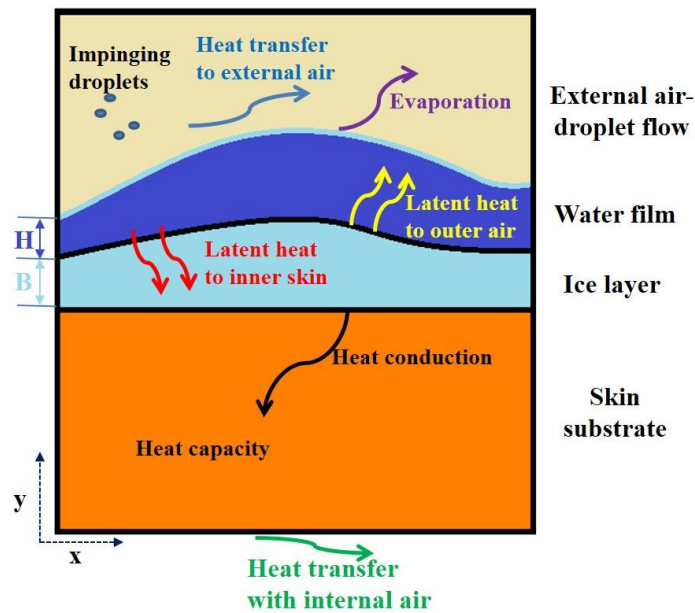


Figure 1. Unsteady thermodynamic model of ice accretion considering solid skin heat conduction.

When the ice layer and the water film on the skin are both thin, the heat transfer processes of them are assumed as quasi-steady to simplify the problem, and the lateral conductions in the water and ice domains are neglected¹³. Therefore, the governing equation for the heat transfer in the water film and ice layer can be written as:

$$\frac{\partial^2 T}{\partial y^2} = 0 \quad (3)$$

Where y is the distance in the normal direction.

The bottom of the ice layer is closely attached with the outer skin surface, so that the temperature and heat flux at the ice-skin interface are continuous. A loosely coupled iterative method is applied for the solution of the solid domain and the icing domain at each time step. The specific method and solution procedure will be described in detail in Section 2.3. Since the surface temperature calculated by the heat conduction equation of the solid skin is extracted to obtain the ice accretion rate and the heat flux at the bottom of the ice layer, the solution of the icing thermodynamic model is based on the constant temperature distribution at the ice-skin interface, which is similar to the traditional Myers' model.

The impinging droplets freeze at the water film-ice layer interface at the phase transition temperature, releasing the latent heat. The latent heat flux through ice layer to the inner skin Q_{inner} is:

$$Q_{\text{inner}} = k_{\text{ice}} \left. \frac{\partial T}{\partial y} \right|_{\text{ice}} = k_{\text{ice}} \frac{T_{\text{ref}} - T_s}{B} \quad (4)$$

Where k_{ice} is the thermal conductivity of ice, T_{ref} is the phase transition temperature of 273.15 K, T_s is the temperature at the ice-skin interface, and B is the thickness of the ice layer.

The latent heat flux through water film to the outer air Q_{outer} is:

$$Q_{outer} = -k_{water} \left. \frac{\partial T}{\partial y} \right|_{water} = -k_{water} \frac{T_{ref} - T_{top}}{H} \quad (5)$$

Where the k_{water} is the thermal conductivity of water, T_{top} is the temperature at the water-air interface, and H is the thickness of the water film. T_{top} is determined by the energy conservation between the water film and the surrounding air-droplet flow. Based on Myers' model, the heat fluxes through the water film-air interface include¹³: 1) air convective heat flux Q_c , 2) evaporative heat flux Q_e (mass loss of water is neglected), 3) sensible heat brought by the impinging droplets Q_d , 4) kinetic energy of the impinging droplets Q_k , 5) aerodynamic heating Q_a . They can be obtained by the following equations¹³:

$$Q_c = h(T_{top} - T_a) = q_c(T_{top} - T_a) \quad (6)$$

$$Q_e = \chi e_0(T_{top} - T_a) = q_e(T_{top} - T_a) \quad (7)$$

$$Q_d = \dot{m}_{imp} \cdot c_w(T_{top} - T_a) = q_d(T_{top} - T_a) \quad (8)$$

$$Q_k = \dot{m}_{imp} \cdot V^2/2 \quad (9)$$

$$Q_a = r \cdot h \cdot V^2/2c_a \quad (10)$$

Where h is the air convective heat transfer coefficient, T_a is the ambient air temperature, q is intermediate variable just for calculation, χ is the evaporation coefficient, e_0 equals 27.03, c_w is the specific heat capacity of water, V is the freestream velocity, r is the recovery factor, c_a is the specific heat capacity of air, and \dot{m}_{imp} is the water droplet impinging rate, which can be obtained by²⁵:

$$\dot{m}_{\text{imp}} = \beta \cdot V \cdot LWC \quad (11)$$

Where β is the droplet collection efficiency, and LWC is the liquid water content.

Then Eq. 5 can be derived as¹³:

$$Q_{\text{outer}} = -k_{\text{water}} \frac{Q_a + Q_k - (q_c + q_d + q_e)(T_{\text{ref}} - T_a)}{k_{\text{water}} + H(q_c + q_d + q_e)} \quad (12)$$

Therefore, the total heat dissipation capacity can be defined as:

$$Q_{\text{ice_cap}} = Q_{\text{outer}} + Q_{\text{inner}} = k_{\text{ice}} \frac{T_{\text{ref}} - T_s}{B} - k_{\text{water}} \frac{Q_a + Q_k - (q_c + q_d + q_e)(T_{\text{ref}} - T_a)}{k_{\text{water}} + H(q_c + q_d + q_e)} \quad (13)$$

When the heat dissipation capacity is greater than the latent heat released by impinging droplets, all the water would freeze and there would be no liquid water film on the skin surface, which means the ice type is rime. In this case, the heat transfer flux through the ice layer to the inner skin is:

$$Q_{\text{inner}} = k_{\text{ice}} \frac{T_{\text{top}} - T_{\text{sub}}}{B} \quad (14)$$

Since the ice layer would exchange heat with the external air directly at the rime ice case, Eq. 14 could be expressed as:

$$Q_{\text{inner}} = k_{\text{ice}} \frac{Q_a + Q_k + i_{\text{sl}} \cdot \dot{m}_{\text{imp}} - (q_c + q_d + q_e)(T_s - T_a)}{k_{\text{ice}} + B(q_c + q_d + q_e)} \quad (15)$$

Where i_{sl} is the latent heat of water condensation.

It can be found that the ice accretion rate is determined by the droplet impinging rate and the total heat dissipation flux. From Eq. 13, the ice layer thickness could not be 0. Therefore, solution algorithm needs special treatment, since there is always no ice layer on the skin at the initial state. In the traditional Myers' model, it is assumed that rime ice forms when droplet impinges on the skin surface to avoid the above problem, and glaze ice would form only when the ice layer grows to a certain extent¹³.

Since the time discretization scheme is explicit, this classic model could not deal with the case when glaze ice or liquid water film forms at the 1st time step, and the constant surface temperature should be changed to a cooling condition to consider this situation¹⁵. Furthermore, the variation of the skin surface temperature T_s is not considered in the traditional model.

In the present work, since there is no heat source in the skin, the ice layer is always formed when droplets impinge on the surface under icing conditions, ignoring the case that only liquid film exists. Considering that it is difficult to change boundary condition of the outer skin surface for the icing thermodynamic model, an implicit time discretization scheme is used to avoid the problem of $B=0$ at the 1st time step, improving the robustness. To start the algorithm, it is firstly assumed that at the current time step, all the water in the control volume, including the liquid water at the last time step and the mass flow of the impinging droplets at this time step, would freeze, and the outer surface of the ice layer is at the freezing temperature. Then, the ice thickness at the current time step can be obtained by:

$$B^i = B^{i-1} + (H^{i-1} \cdot \rho_w + \dot{m}_{\text{imp}} \cdot \Delta t) / \rho_{i_r} \quad (16)$$

Where ρ_w is the water density, ρ_{i_r} is the rime ice density (880 kg/m³).

From Eq. 13, the total heat dissipation capacity in this condition is:

$$Q_{\text{ice_cap}}^i = k_{\text{ice}} \frac{T_{\text{ref}} - T_s^i}{B^i} - Q_a - Q_k + (q_c + q_d + q_e)(T_{\text{ref}} - T_a) \quad (17)$$

Then the heat dissipation capacity is compared with the latent heat to validate or amend the assumption that all water freezes. If the heat dissipation capacity is greater than the latent heat flux at this time step, which is expressed as:

$$Q_{\text{ice_cap}}^i > i_{\text{sl}}(n\dot{\lambda}_{\text{imp}} + H^{i-1} \cdot \rho_w / \Delta t) \quad (18)$$

All the liquid water would freeze as rime ice, and the water film thickness $H^i=0$.

The ice layer thickness B^i is obtained by Eq. 16, and the heat flux through the ice layer to the inner skin is:

$$Q_{\text{inner}}^i = k_{\text{ice}} \frac{Q_a + Q_k + i_{\text{sl}}(n\dot{\lambda}_{\text{imp}} + H^{i-1} \cdot \rho_w / \Delta t) - (q_c + q_d + q_e)(T_s^i - T_a)}{k_{\text{ice}} + B^i(q_c + q_d + q_e)} \quad (19)$$

If the total heat dissipation capacity is less than the latent heat flux, Eq. 18 would not hold, and part of the water would freeze as glaze ice with the rest remaining liquid. However, since the surface temperature changes with time, the heat dissipation capacity varies. The liquid water at the last time step might freeze, or the ice layer might melt at this time step. Therefore, unlike the traditional Myers' model, the thicknesses of the water film and ice layer could increase or decrease with time. These thicknesses and the actual heat dissipation flux Q_{dis} at the current time step are calculated by:

$$\begin{cases} Q_{\text{dis}}^i = k_{\text{ice}} \frac{T_{\text{ref}} - T_s^i}{B^i} - k_w \frac{Q_a + Q_k - (q_c + q_d + q_e)(T_{\text{ref}} - T_a)}{k_w + H^i(q_c + q_d + q_e)} \\ B^i = B^{i-1} + Q_{\text{dis}}^i \cdot \Delta t / (\rho_{\text{i_g}} \cdot i_{\text{sl}}) \\ H^i = H^{i-1} + (n\dot{\lambda}_{\text{imp}} - Q_{\text{dis}}^i / i_{\text{sl}}) \Delta t / \rho_w \end{cases} \quad (20)$$

Where $\rho_{\text{i_g}}$ is the glaze ice density (917 kg/m³).

Under this condition, the heat flux through the ice layer to the inner skin is obtained by:

$$Q_{\text{inner}}^i = k_{\text{ice}} \frac{T_{\text{ref}} - T_s^i}{B^i} \quad (21)$$

It can be seen from the established thermodynamic model that when the skin

temperature variation is neglect, the thicknesses of both ice layer and water film would only increase over time, and the present model would regress to the traditional Myers' model.

2.3 Solution Procedure

The icing process is determined by both the water film phase transition and the skin heat conduction, of which the governing equations need to be coupled and iteratively solved. The simulation is implemented by the commercial CFD software ANSYS FLUENT - 18.1 with its user-defined functions (UDFs)²⁶. The solution procedure is shown in Figure 2.

To initialize the simulation, the skin temperature is set as the ambient value, and the thicknesses of both water film and ice layer are 0. At a certain time step, the solution of the skin heat conduction is obtained by the finite volume solver of FLUENT, and provides the outer skin surface temperature T_s^i as an input condition for the icing thermodynamic model. Firstly, the total heat dissipation capacity at this time step is calculated by Eq. 17 according to T_s^i . Then, the ice type, rime ice or glaze ice, is determined using Eq. 18. At last, the phase transition equations are solved, and the heat flux at the ice-skin interface Q_{inner}^i is obtained to serve as a Neumann boundary condition for the solid skin heat conduction. The calculation continues iteratively until the temperature difference between two iterations is small enough, which indicates the coupled calculation of the current time step reaches convergence. The parameters such as skin temperature distribution, thicknesses of water film and ice layer are saved, and then the solution of the next time step begins until the end of the simulation time.

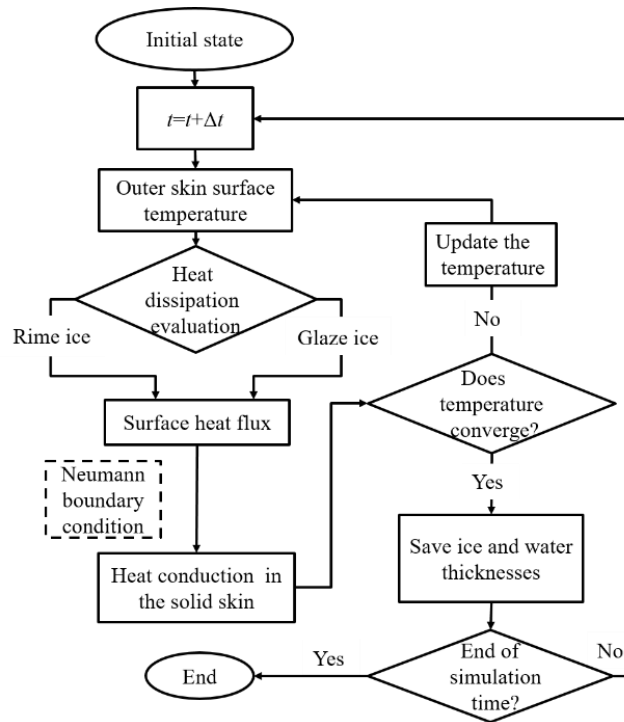


Figure 2. Flow chart of the solution procedure for the coupled ice accretion simulation.

3 Geometry and Boundary Conditions

To test the present model and study the conjugate heat transfer process, a rectangular skin segment is selected to conduct ice accretion simulations as shown in Figure 3. The width and thickness of the segment are 30 mm and 3 mm, respectively. The upper surface is the outer skin surface adjacent to the external air-droplet domain, while the bottom of the skin segment is close to the internal air. The upper surface is divided into two halves, naming left zone and right zone. During the simulations, the water droplets can be set to impinge on the left zone or on both zones. The boundary conditions for the heat exchange with the external air-droplet flow are as follows¹³: the air velocity is 90 m/s in the x direction, the collection efficiency is 0.55, *LWC* is 1

g/m^3 , the air convective heat transfer coefficient is $500 \text{ W/m}^2/\text{K}$, and the air temperatures of 263.15 K and 270 K are selected for the simulations.

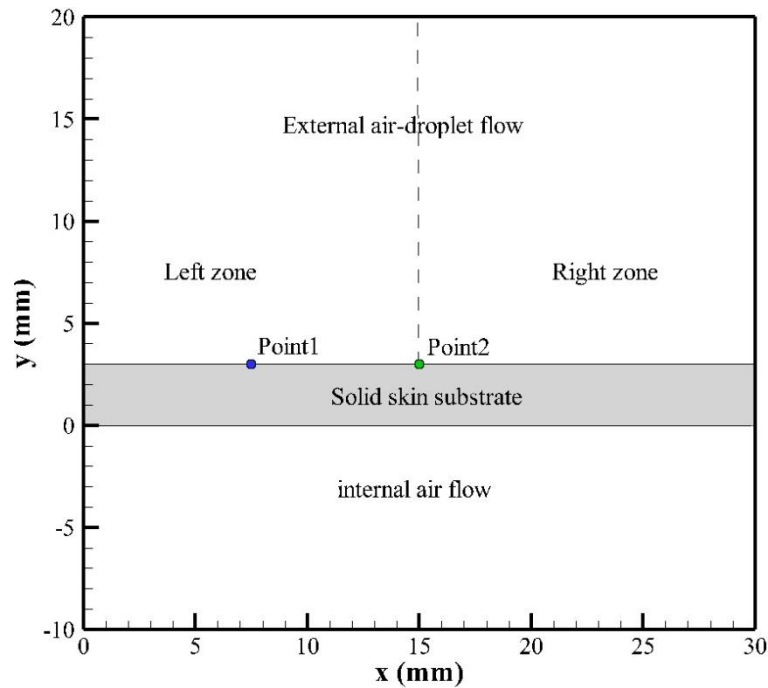


Figure 3. Geometry of the skin segment.

The material of the skin substrate is uniform, and aluminum and steel are applied in different simulation cases to study the effects of material property on icing characteristics. It can be seen from Table 1 that the thermal conductivities of the two metals are very different. The two side faces of the segment are set as adiabatic boundary. Generally, there is an air gap inside the aircraft skin, thus the inner surface of the skin is in natural convection with the internal air flow. Besides constant air temperature condition following the traditional Myers' model, a Neumann boundary condition with the natural convective heat transfer coefficient of $10 \text{ W/m}^2/\text{K}$ is used there, and the reference temperature is the same with the external air. In addition, other parameters, such as properties of air, water and ice, can be found in Ref. 13. At

the initial state, the temperature of skin is set as the same with that of the external air, and the thicknesses of the water film and ice layer is 0.

Table 1. Material properties of the skin substrate.

Material	Conductivity (W/m/K)	Density (kg/m³)	Specific heat capacity (J/kg/K)
Aluminum	202.4	2719	871
Steel	16.27	8030	502.48

4 Results and Discussion

4.1 Model Validation

To validate the present model, two icing cases ($T_a=263.15$ K and 270 K) are simulated, and in those cases the skin temperature is set constant to meet the requirement of Myers' model. Droplets impinge on both left and right zones of the skin, and the other boundary conditions are listed in Section 3. The simulated water film thickness H and ice layer thickness B are shown in Figure 4. Since the skin temperature is lower than the freezing point of water, at the early stage of icing, once the super-cooled droplet impinges on the surface, it freezes and the latent heat is dissipated through convection to air and conduction to skin, and the ice layer grows at its maximum rate. As ice layer grows, its heat conduction resistance increases. When the heat dissipation capacity is not strong enough to cover all the latent heat of water freezing, part of the droplets remain liquid, and the ice type evolves as glaze ice. As the heat conduction resistance increases, the icing rate decreases.

Comparing the two temperature cases, the heat dissipation capacity of case 263.15 K is stronger than that of case 270 K, therefore the transition time from rime ice to glaze ice of the former case is greater than that of the latter one, and its ice layer thickness is also greater. The difference in curve $B+H$ of the two cases is due to that the density of rime ice is greater than that of glaze ice. In addition, the results of the present model match well with those obtained by Myers' model, which validates the present unsteady thermodynamic model.

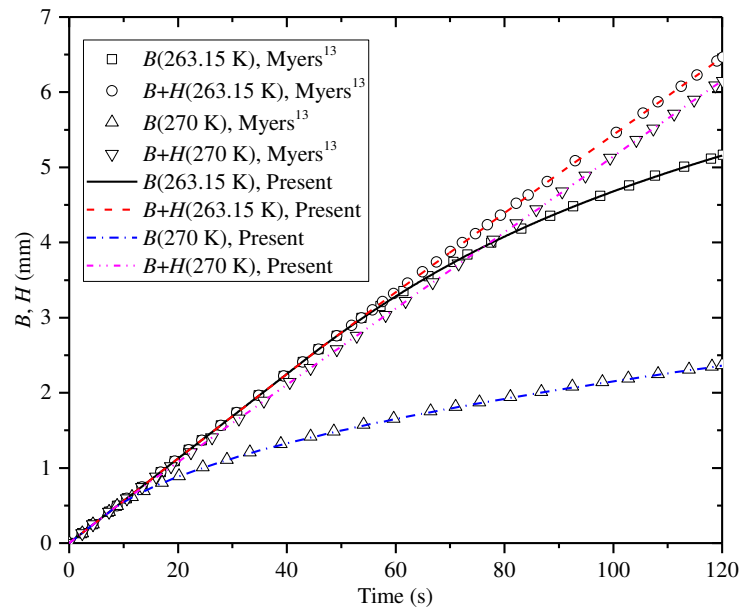


Figure 4. Validation case results: thicknesses of ice layer and water film.

4.2 Effect of Time Step

To analyze the effect of time step on the unsteady ice accretion simulation, three cases are calculated with droplet impinging on all the upper skin surface, in which the time steps are 1 s, 0.5 s, and 0.25 s, respectively. The effect of the skin heat conduction is included, and the inner skin surface is in natural convection with the internal air. Figure 5 and Figure 6 show the results of the skin surface temperature and

the ice thickness. The curves of three cases show little difference. Only at the transition range from rime ice to glaze ice, a smaller time step could lead to a more precise description of the transition process. The comparison indicates that the present model is not sensitive to the selection of time step, since its time discretization scheme is implicit. The time step of 1 s would be applied in the following simulations.

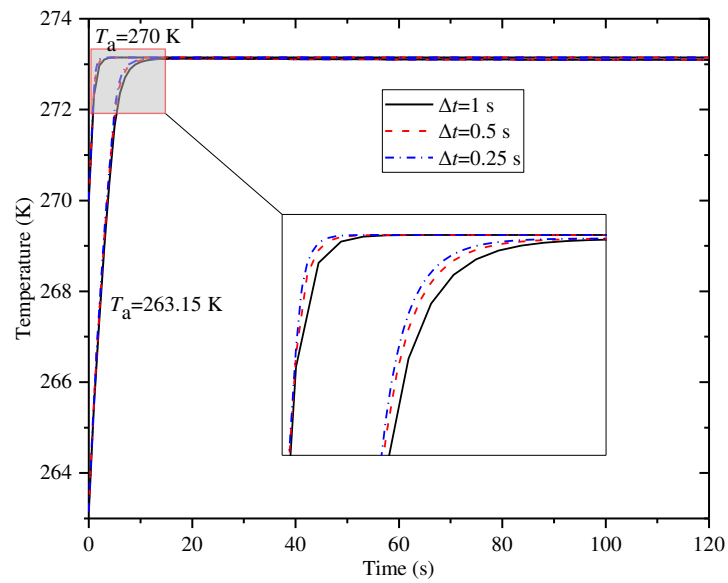


Figure 5. Time step case results: skin surface temperature.

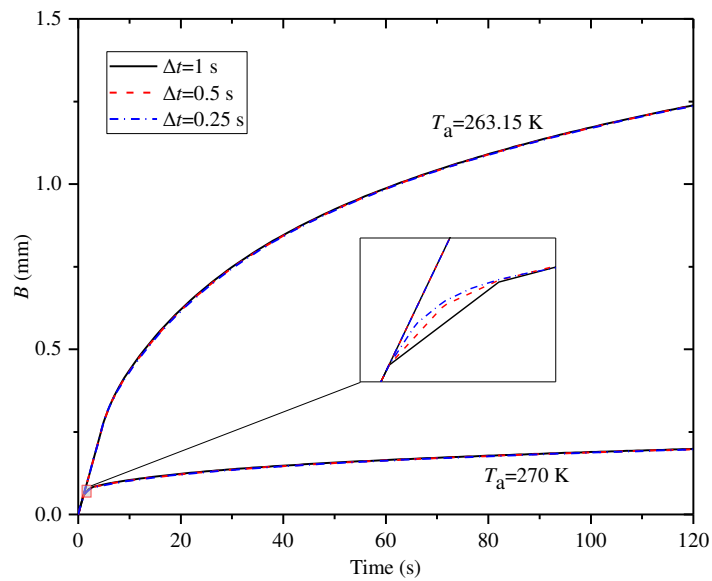


Figure 6. Time step case results: ice layer thickness.

4.3 Effect of Skin Normal Heat Conduction

Icing cases are simulated with the present model considering the normal heat conduction of the skin substrate, and the results of ice layer thickness are compared with those of Myers' model in which the skin heat conduction is neglected (the skin temperature is constant). In the present model, the boundary condition of the inner skin surface is set as constant temperature and natural convective heat transfer, respectively. The aluminum skin is used in the icing simulations. The results at $T_a=263.15$ K and $T_a=270$ K are shown in Figure 7, Figure 8, and Figure 9.

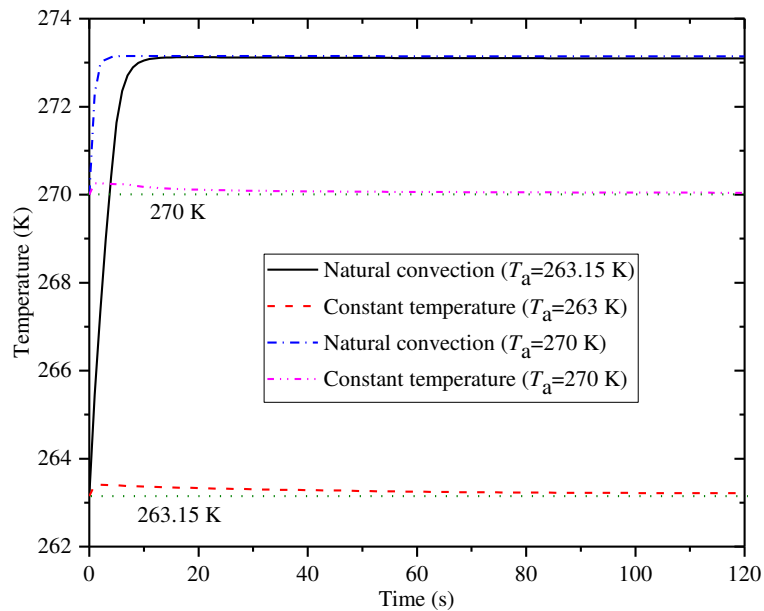


Figure 7. The outer skin surface temperatures under different boundary conditions.

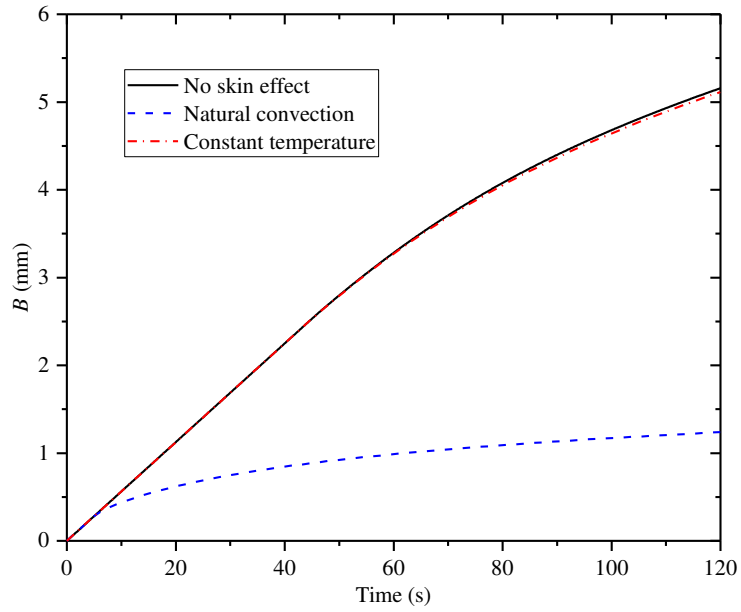


Figure 8. Results of the ice layer thickness at $T_a=263.15$ K.

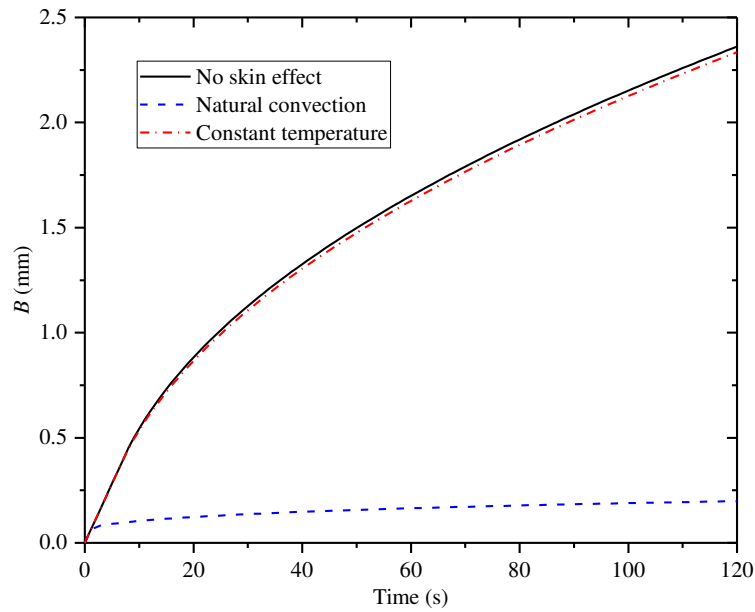


Figure 9. Results of the ice layer thickness at $T_a=270$ K.

In the case that the inner skin surface is at constant temperature, the outer skin surface temperature increases at the early stage, then decreases slowly and tends to the constant temperature of the inner surface as shown in Figure 7. The reason is that the latent heat released by water freezing conducts to the skin, and increases the skin

temperature. As the ice layer grows, the heat conduction declines. Comparing with the result of Myers' model, the ice layer thickness at rime ice region is consistent, while at glaze ice region, the ice layer thickness of the present model is smaller than Myers' (see Figure 8 and 9), since the introduction of the skin normal heat conduction weakens the heat dissipation to the internal air. The transition from rime ice to glaze ice becomes earlier, and the ice layer is a little thinner as the heat resistance of the skin is small in the normal direction.

In the case that the inner skin surface boundary is natural convection, the results show significant divergence with those of Myers' model at the air temperatures of both 263.15 K and 270 K. In this case, the heat resistance from ice layer to internal air flow is large, therefore the skin temperature increases rapidly to the phase transition temperature of 273.15 K due to the latent heat of water freezing, and the substantial thermal capacitance associated with the skin would vanish at the very early stage of icing. Since the heat dissipation is restricted by the inner surface convection, the ice type would transition from rime ice to glaze ice rapidly, and the ice layer grows slowly.

In general, the normal heat conduction has slight influence on the icing process, but the boundary condition of the inner skin surface would strongly affect the heat dissipation to the inner skin and the skin temperature distribution. The outer skin surface temperature in turn affects the heat dissipation, ice type, and ice layer thickness. The icing process is conjugate with the unsteady solid skin heat conduction.

4.4 Effect of Skin Lateral Heat Conduction

Considering that the external air-droplet condition along the wing surface could be non-uniform, water droplets might impinge on only part of the wing. In this section, the cases are simulated in which water droplet impingement only occurs in the left zone (see Figure 3) to discuss the effects of the skin lateral heat conduction on the icing process. The right zone of the aluminum skin substrate is exposed to the dry air convection, and the boundary condition of all the inner skin surface is natural convection.

Figure 10 shows the temperature variation of the outer skin surface with time at the air temperature of 263.15 K. The surface temperature of the left zone rises immediately from the initial value as a result of the latent heat released by water freezing. Then, due to the lateral heat conduction from the left zone, the right zone temperature rises, and the temperature difference between the left and right zones narrows over time. After about 20 s, the surface temperature reaches its maximum. Then, it decreases and tends to be stable. This is due to two reasons: first, the growth of the ice layer hinders the heat transfer across the skin substrate at the left zone; second, the rise of the skin temperature, especially the surface temperature of the right zone, enhances the convective heat loss to air. Similar phenomenon that the surface temperature first increased then decreased was found in glaze icing experiment²¹, and it was explained to be caused by that the ice roughness enhanced the convection. From the present discussion, the lateral heat conduction might be another reason.

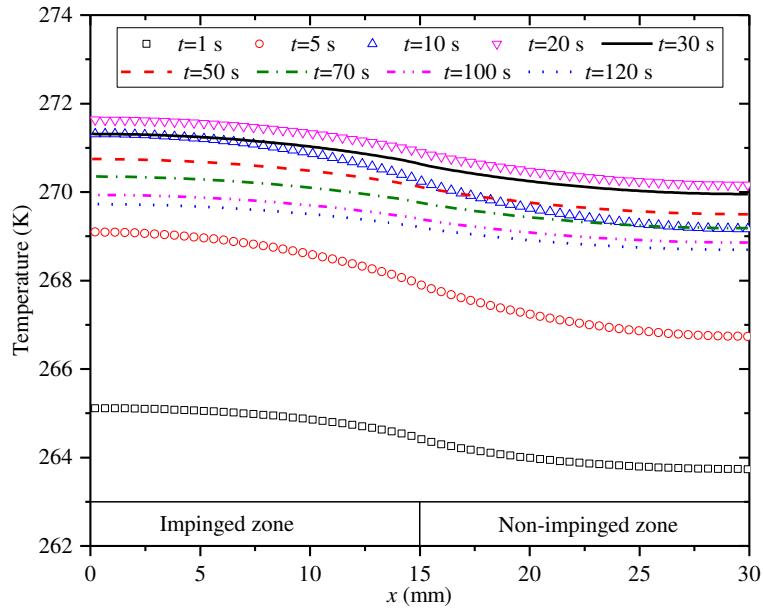


Figure 10. Distributions of outer skin surface temperature at different time instants ($T_a=263.15$ K, aluminum).

Figure 11 shows the temperature contour of the skin substrate when the temperature is stable at $t=120$ s. The lateral temperature gradient at the interface of the impinged and non-impinged zones is the largest, and decreases as it goes to the two sides of the skin. The heat flux enters the skin through the left outer surface, and dissipates through the right surface, therefore the lateral temperature gradient is larger at the outer surface (upside) than at the inner surface (downside).

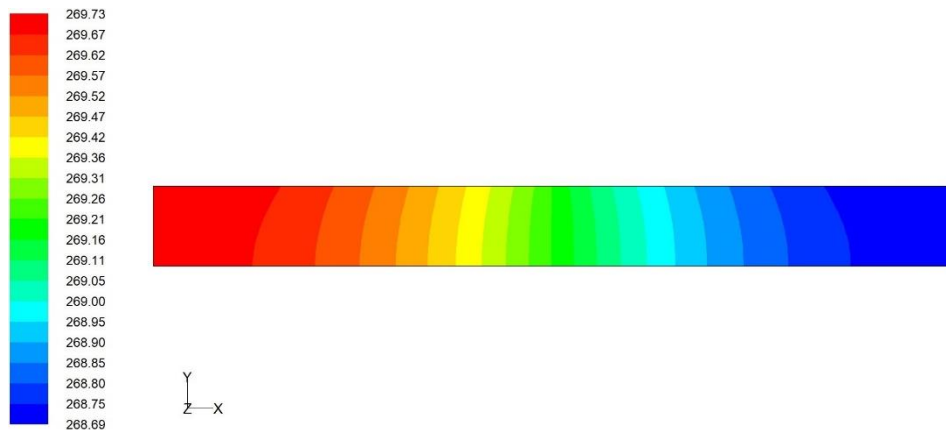


Figure 11. Temperature contour (K) of the skin substrate at $t=120$ s.

The ice layer growth process is shown in Figure 12. At the early stage, the skin temperature is low and the impinging droplets freeze as rime ice. Since the heat is transferred from left to right in the skin, the temperature of left side of the impinged zone ($x=0$ mm) is higher than the rest of the area over time. Therefore, the heat dissipation to the inner skin there is weaker, glaze ice forms earlier, and the icing rate is smaller. At the right side of the impinged zone ($x=15$ mm), the temperature is lower than the left side due to the heat dissipation of the non-impinged zone, thus the transition from rime ice to glaze ice is later, and the ice thickness is greater. Due to the lateral temperature difference, the icing rate of the left side is always smaller than the right side in the impinged zone. This trend is more obvious in the case of 270 K (Figure 13). A higher ambient temperature leads to an earlier transition to glaze ice, and the icing rate difference between the left and right sides of the impinged zone is more notable.

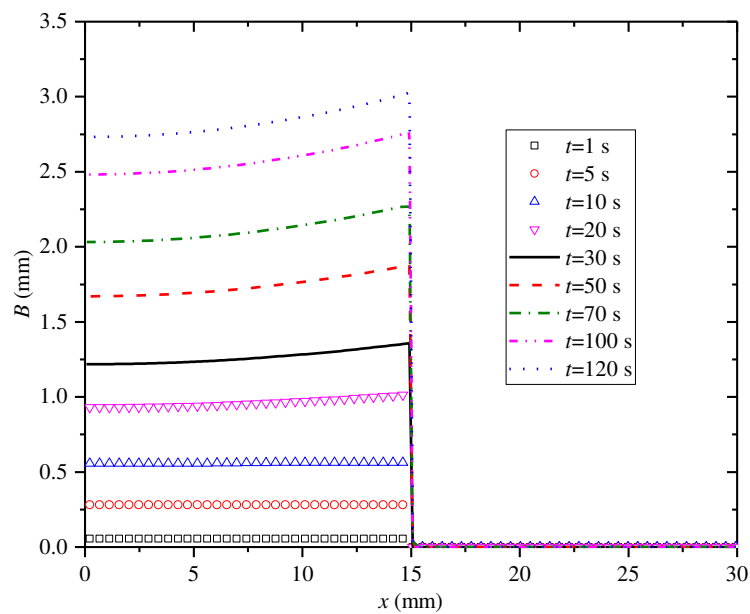


Figure 12. Distributions of ice layer thickness at different time instants ($T_a=263.15$ K, aluminum).

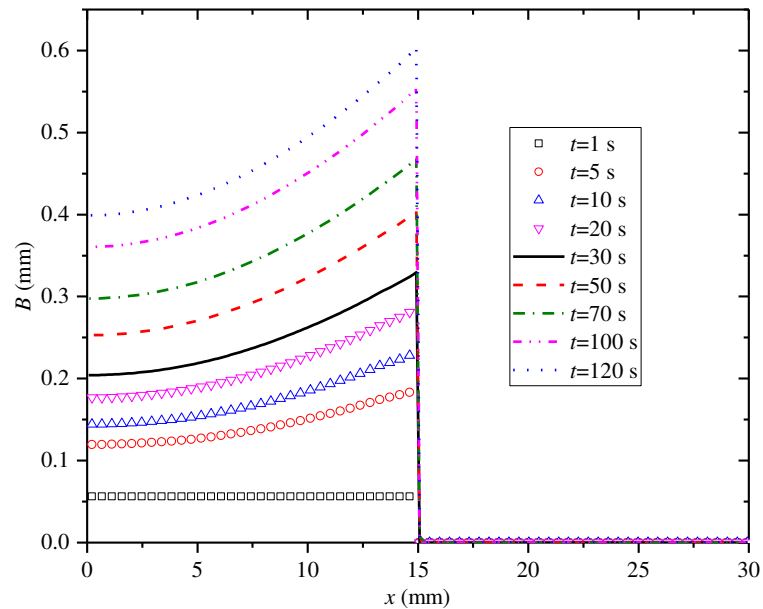


Figure 13. Distributions of ice layer thickness at different time instants ($T_a=270$ K, aluminum).

Comparing Figure 12 and Figure 13 with Figure 8 and Figure 9, the ice layer thicknesses here are larger than those only considering normal heat conduction at the same time instants, but smaller than those of which the skin is at constant temperature. This is due to that the lateral heat conduction leads to a re-distribution of skin temperature. Therefore, to simulate the icing process more accurately, the skin heat conduction needs to be considered, instead of simply setting an adiabatic or a constant-temperature boundary.

4.5 Effect of Skin Material Property

In the above cases, the skin material is set as aluminum. In this section, the case with the skin material of steel is simulated, and the ambient air temperature is 263.15

K. As in Section 4.4, the droplet impingement only occurs at the left zone. The results of the outer skin surface temperature and ice layer thickness are shown in Figure 14 and Figure 15, respectively. Comparing with the aluminum case (Figure 10 and Figure 12), the conductivity of steel is less, so that the lateral skin heat conduction to the right side is weaker as well as the latent heat dissipation of water to the inner skin. The temperature increase of the left zone is more rapid, while that of the right zone is slower, leading to a larger lateral temperature difference. Therefore, the transition point to glaze ice is earlier than the aluminum case, and the ice layer thickness distribution is more uneven. In most of the area, the ice layer thickness is smaller than that of the aluminum case, but the value is greater at $x=15$ mm (the interface of the impinged and non-impinged zones, Point 2 in Fig. 3), since the lateral heat conduction is weaker and the local temperature is lower at this location. In addition, the temperature variation of the skin is similar with the aluminum case, which means the temperature increases at first then decreases. But the decrease rate is smaller due to larger thermal resistance of steel, especially at the right zone, the surface temperature increases to its maximum without any decline.

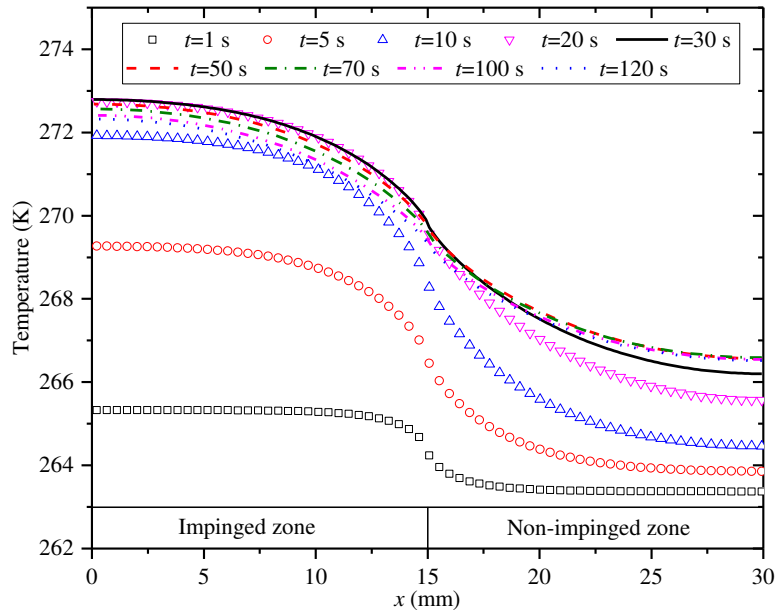


Figure 14. Distributions of outer skin surface temperature at different time instants ($T_a=263.15$ K, steel).

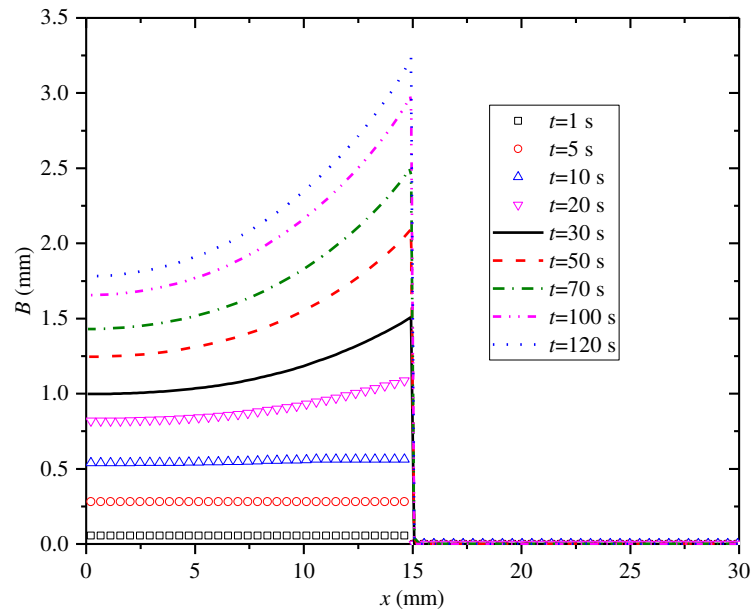


Figure 15. Distributions of ice layer thickness at different time instants ($T_a=263.15$ K, steel).

Figure 16 and Figure 17 show the temperature and ice layer thickness variation at $x=7.5$ mm (the middle of the left zone, Point 1 in Fig. 3) and $x=15$ mm (the edge of

the impinged zone, Point 2 in Fig. 3) with different materials when $T_a=263.15$ K. The temperatures of both locations increase rapidly and then decrease gradually with time. The speed and amplitude of the temperature change of the aluminum skin are greater than those of the steel skin. The ice thicknesses of both materials are consistent at the rime ice stage, and the deviation appears at the glaze ice stage when the growth rate of the ice thickness is slower. Due to the heat dissipation of the non-impinged zone, the temperature at $x=15$ mm is always lower than that at $x=7.5$ mm, so that the ice thickness there is greater.

At $x=7.5$ mm, the surface temperature of the steel skin is higher than that of the aluminum skin all the time, while its ice thickness is thinner and the thickness difference tends to increase over time. At $x=15$ mm, the surface temperature of the aluminum skin changes more rapidly than that of the steel skin with higher peak value. After decreasing at a higher speed, the surface temperature of the aluminum skin becomes lower than that of the steel skin. The ice layer thickness of the aluminum skin is smaller than that of the steel case, but the difference tends to decrease over time. To sum up, the ice accretion process would not only be affected by the material property of the skin substrate, but the icing characteristics could also differ at various locations.

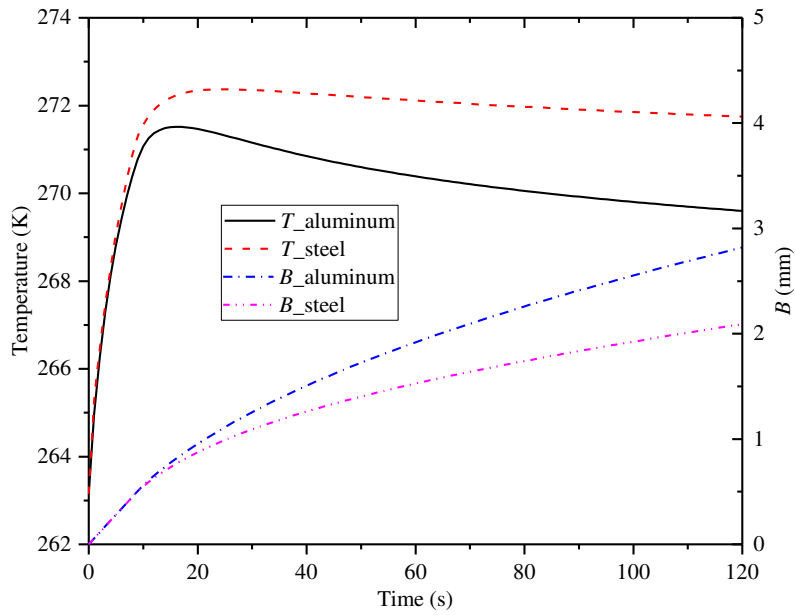


Figure 16. Results of surface temperature and ice layer thickness at $x=7.5$ mm.

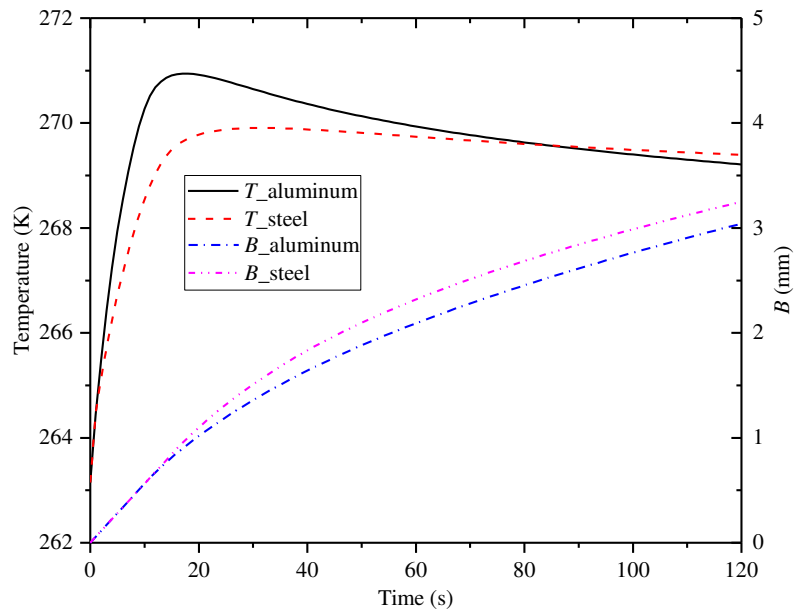


Figure 17. Results of surface temperature and ice layer thickness at $x=15$ mm.

Conclusions

A conjugate thermodynamic model of aircraft ice accretion process was established to consider the phase transition of icing and the unsteady solid conduction simultaneously, and a corresponding time-implicit solution algorithm was developed.

Icing cases of 2-D skin were numerically studied to obtain the variations of temperature and water film/ ice layer thickness over time, and the effects of solid heat conduction on icing characteristics were analyzed. The conclusions are as follows:

1) In the simplified case where the skin substrate is at constant temperature, the result of present model matches well with that of Myers' model. And the present model and solution algorithm are not sensitive to the selection of time step.

2) The normal skin heat conduction would slightly affect the icing process with constant temperature as the inner skin surface boundary, but when the natural convection boundary condition is used, the skin temperature increases more rapidly and the ice layer thickness grows more slowly.

3) Considering the lateral heat conduction of the skin substrate, the skin temperature increases firstly then decreases, explaining the phenomenon observed in the experiment. In addition, due to the lateral heat conduction, the icing rate is uneven, and the value near the dry zone is greater than that on other impinged surface.

4) A smaller heat conductivity of the skin substrate leads to a larger lateral temperature gradient and a smaller temperature variation over time, and the icing rate is generally smaller and more uneven. The peak ice thickness with smaller heat conductivity could be even larger than that with higher heat conductivity.

5) The water film runback has not been considered in the present icing model, and it will be studied in future research to analyze the effect of heat conduction on the heat and mass transfer process of ice accretion.

Funding

This work was supported by the National Natural Science Foundation of China (No. 51806008), and the National Numerical Wind Tunnel Project (No. NNW2019ZT2-A07).

References

1. Cao Y, Tan W, Wu Z. Aircraft icing: An ongoing threat to aviation safety. *Aerospace Science and Technology* 2018; 75: 353-385.
2. Yu J, Peng L, Bu X, Shen X, Lin G, Bai L. Experimental investigation and correlation development of jet impingement heat transfer with two rows of aligned jet holes on an internal surface of a wing leading edge. *Chinese Journal of Aeronautics* 2018; 31(10): 1962–1972.
3. Shen X, Wang H, Lin G, Bu X, Wen D. Unsteady simulation of aircraft electro-thermal deicing process with temperature-based method. *Proceedings of the Institution of Mechanical Engineers - Part G: Journal of Aerospace Engineering* 2020; 234(2): 388-400.
4. Jones SM, Reveley MS, Evans JK. Subsonic Aircraft Safety Icing Study. NASA/TM-2008-215107, 2008.
5. Wright WB. User manual for the NASA Glenn ice accretion code LEWICE version 2.2.2. NASA-CR-2002-211793, 2002.
6. Fouladi H, Habashi WG. FENSAP-ICE Modeling of Ice Accretion on a Helicopter Fuselage in Forward Flight. AIAA paper, no. 2012-2674, 2012.
7. Hedde T, Guffond D. ONERA Three-Dimensional Icing Model. *AIAA Journal* 1995;

33(6): 1038-1045

8. Gent RW. TRAJICE2 - A Combined Water Droplet Trajectory and Ice Accretion Prediction Program for Aerofoils. Royal Aerospace Establishment. Technical Report 90054, 1990.

9. Fortin G, Perron J, Mingione G, Luliano E. CIRAAMIL ice accretion code improvement. AIAA paper, no. 2009-3968, 2009.

10. Messinger BL. Equilibrium temperature of an unheated icing surface as a function of air speed. *Journal of the Aeronautical Sciences* 1953; 20(1): 29-42.

11. Shen X, Lin G, Yu J, Bu X, Du C. Three-Dimensional Numerical Simulation of Ice Accretion at the Engine Inlet. *Journal of Aircraft* 2013; 50(2): 635-642.

12. Bourgault Y, Beaugendre H, Habashi WG. Development of a Shallow-Water Icing Model in FENSAP-ICE. *Journal of Aircraft* 2000; 37(4): 640-646.

13. Myers TG. Extension to the Messinger Model for Aircraft Icing. *AIAA Journal* 2001; 39: 211-218.

14. Brakel TW, Charpin JPF, Myers TG. One-dimensional ice growth due to incoming supercooled droplets impacting on a thin conducting substrate. *International Journal of Heat and Mass Transfer* 2007; 50: 1694-1705.

15. Myers TG, Hammond DW. Ice and Water Film Growth from Incoming Supercooled Droplets. *International Journal of Heat and Mass Transfer* 1999; 42: 2233-2242.

16. Myers TG, Charpin JPF. A mathematical model for atmospheric ice accretion and water flow on a cold surface. *International Journal of Heat and Mass Transfer* 2004; 47: 5483-5500.

17. Du Y, Gui Y, Xiao C, Yi X. Investigation on heat transfer characteristics of aircraft

icing including runback water. *International Journal of Heat and Mass Transfer* 2010; 53: 3702-3707.

18. Cao Y, Hou S. Extension to the Myers Model for Calculation of Three-Dimensional Glaze Icing. *Journal of Aircraft* 2015; 50(1): 106-116.

19. Kong W, Liu H. Unified icing theory based on phase transition of supercooled water on a substrate. *International Journal of Heat and Mass Transfer* 2018; 123: 896–910.

20. Gao L, Liu Y, Hu H, An experimental investigation of dynamic ice accretion process on a wind turbine airfoil model considering various icing conditions. *International Journal of Heat and Mass Transfer* 2019; 133: 930-939.

21. Li L, Liu Y, Zhang Z, Hu H. Effects of thermal conductivity of airframe substrate on the dynamic ice accretion process pertinent to UAS inflight icing phenomena. *International Journal of Heat and Mass Transfer* 2019; 131: 1184-1195.

22. Morency F, Tezok F, Paraschivoiu I. Heat and mass transfer in the case of anti-icing system simulation. *Journal of Aircraft* 2000; 37(6): 245–252.

23. Shen X, Guo Q, Lin G, Zeng Y, Hu Z. Study on Loose-Coupling Methods for Aircraft Thermal Anti-Icing System. *Energies* 2020; 13, 1463.

24. Chauvin R, Villedieu P, Trontin P. A robust coupling algorithm applied to thermal ice protection system unsteady modeling. 6th AIAA Atmospheric and Space Environments Conference – AVIATION 2014; Jun 2014, ATLANTA, United States.

25. Shen X, Liu X, Lin G, Bu X, Wen D. Effects of Anisotropic Composite Skin on Electro-thermal Anti-icing System. *Proceedings of the Institution of Mechanical Engineers - Part G: Journal of Aerospace Engineering*, 2019; 233(14): 5403–5413.

26. *ANSYS FLUENT User's Guide*. release 18.0. ANSYS, Inc; 2018.